DEM investigation of shear mobilisation during tyre strip pull-out test

Zeng-Le Ren[1*], Yi Pik Cheng[2], Xiaomin Xu[3], Lihua Li[4]

[1]*Research Associate, Guangdong Provincial Key Lab of Robotics and Intelligent System, Shenzhen Institute of Advanced Technology , Chinese Academy of Sciences, Shenzhen, 518055, China, E-mail: zl.ren1@siat.ac.cn (corresponding author)*
[2]*Associate Professor, Department of Civil, Environmental and Geomatic Engineering, Chadwick Building, University College London, Gower Street, London WC1E 6BT, United Kingdom, E-mail:*yi.cheng@ucl.ac.uk
[3]*Research Associate, Department of Engineering, University of Cambridge, 7a JJ Thomson Avenue, Cambridge, UK, CB3 0FA, United Kingdom, E-mail:* xx787@cam.ac.uk
[4]*Professor, School of Civil Engineering, Architecture, and Environment, Hubei University of Technology, Wuhan, 430068, PR China. Email: researchmailbox@163.com*

ABSTRACT:

This paper presents an evaluation of the pull-out behaviour of tyre strip-reinforced granular soil. The three-dimensional discrete element method (DEM) and laboratory testing were used to systematically calibrate the soil particles and the tyre strip based on their stress-strain relationship, tensile stiffness, and interface shear strength. Particle shapes were considered during sand calibration. The scaled pull-out resistance was found to match that of the experimental data. Contributions of the sectional interface shear force to the total pull-out resistance were calculated to explain the progressive failure mechanism mobilised at the tyre-sand interface. The shear force along the tyre strip was not uniformly distributed but higher in the middle portion of the tyre strip. It gradually extended towards the front end of the tyre strip before global interface slipping failure occurred. Comparing the pull-out behaviour of extensible and inextensible tyre strips, the elastic deformation of the tyre strip delayed the occurrence but not the magnitude of peak pull-out force. Micro-mechanical interactions between tyre strip and sand during shear mobilisation were discussed, and induced anisotropy was revealed. The experimental and DEM investigation results in this study provide researchers with an improved understanding of tyre-soil interaction under pull-out loads.

KEYWORDS: Geosynthetics, Rubber tyre strip; 3D Discrete Element Method (DEM); Pull-out behaviour; Shear mobilisation; Micro-analysis

1. INTRODUCTION

Recycled tyres have been successfully used in geotechnical engineering to reinforce granular aggregates as a sustainable and economical solution. The first research on waste tyres reinforced soil was commissioned in 1976, France. Then the first application of waste tyre reinforced structure was built in 1984, France, where a 5 m high by 10 m long retaining wall was constructed (Sayão et al, 2009). Traditionally, waste tyres could be processed into strips, shreds or powder, and then mixed, for example, with soils to reinforce embankments, slopes, retaining walls, foundations and docks (ASTM D6270, 2008). Results of many laboratory tests and some field demonstration projects involving tyre-sand mixtures have been widely reported in the last 20 years, for example, Bosscher et al. (1992,1997), Foose et al. (1996), Humphrey (1998), Ghazavi and Sakhi (2005), Balunain et al. (2014), Bali Reddy et al. (2016), McCartney et al. (2017), Fox et al. (2017), and Manohar & Anbazhagan (2021). Related tyre research had attracted more attention worldwide, especially in the Asia Pacific region and in Europe (Hazarika et al., 2010). Compared with granulated tyre or tyre powder, using a larger size of tyre products like tyre strips could promote industry up-take when considering the processing cost.

For example, studies of a mat-reinforced slope with the mat made of whole tyres and cut tyres, i.e. tyres with one sidewall removed were conducted (O' Shaughnessy and Gaga, 2000). Kim et al. (2011) conducted field-scaled pull-out tests to compare the pull-out performance of cell-type tyre and geocell reinforced soil, respectively. It was concluded that the ultimate pull-out capacity of cell-type waste tyres was about 1.25 times larger than that of geocells. Li et al. (2017) found that the pull-out loads mobilised by tyre strips were two times higher than the pull-out loads mobilised by the uniaxial and biaxial geogrids, under the same pull-out testing conditions. Additional recent studies (Li et al., 2016; Li et al., 2020; Li et al., 2021) also revealed a good potential of using larger-size waste tyres to partially or completely replace geogrids or geocells. However, there is only a limited number of studies that focus on the load-deformation behaviour of tyre strips rather than tyre chips, particularly through pull-out tests. It is therefore essential to investigate further into the interface behaviour between soil and tyre and the pull-out behaviour of tyre

67 embedded in the soil. Better understanding the underlying mechanisms is important for the
68 design of tyre reinforced structures.

69 Since many factors, such as apparatus type, testing conditions, material properties
70 and surface characteristics of the tyre strip and how the mat is produced, etc., affect the
71 interface shear behaviour, the interaction mechanism between soil and tyre becomes fairly
72 complex. To help understand tyre reinforcement mechanisms, some numerical simulations
73 with particular consideration of the discontinuous nature of granular material were
74 proposed to explore tyre-soil interaction, unfortunately, most of them were focused on tyre-
75 soil mixtures. Lee et al. (2014) studied the behaviour of sand - tyre chip mixtures under
76 different strain levels using laboratory tests and two-dimensional numerical simulations and
77 found that the angle of friction increases as the sand fraction increases, and the mixtures
78 show contractive behaviour. The 3D DEM models for rigid-grain and soft tyre chips were
79 proposed to explore the behaviour of sand-tyre mixtures based on triaxial monotonic
80 compression tests and one-dimensional compression tests (Lopera Perez et al., 2016;
81 Asadi et al., 2018; Zhang et al., 2020). These researchers concluded that both tyre size
82 and content should be considered depending on the intended purpose of use for the
83 mixtures. To investigate further the tyre-soil interface behaviour, Ren et al.(2020) proposed
84 specific and convincing details about rubber tyre calibration processes, along with
85 validation and verification using 3D DEM numerical tensile test simulations, with a focus
86 on creating large-size tyre strip models. However, the micro-mechanical tyre strip
87 reinforcement mechanism through numerical pull-out tests has not been investigated.

88 This paper is aimed at addressing the lack of micro investigation of the shear
89 mobilisation between tyre strip and soil based on pull-out tests. Tyre strip of 60 mm to 100
90 mm in length embedded in soil was reproduced by building a series of numerical models
91 based on the well-established contact constitutive models in PFC^{3D} version 5.0 (Itasca,
92 2018). The results of the numerical simulation include the visualization of a load transfer
93 mechanism for both tyre and soil particles assembly, special emphasis was also placed on
94 the inherent changes of interface contact forces that contribute to macroscopic strength as
95 well as the correlation between macro pull-out force and micro anisotropy parameters. The
96 progressive shear mobilisation of the rubber tyre during the pull-out test was also

investigated. The results could help understand the tyre strip reinforcement mechanism and provide a basis to improve the guidance to relevant engineering practice.

2. NUMERICAL MODELLING AND CALIBRATION

2.1 Numerical direct shear tests

Simulation of direct shear tests was performed using DEM to calibrate the micro-mechanical parameters of sand. Fujian standard sand (the uniformity of coefficient was 1.92, the coefficient of curvature was 1.4) was used in the test. Since the computational time in DEM simulations is highly dependent on the number of particles, an 'up-scaling' technique was commonly used to balance the computational cost against the scaling effect on the sample response (Wang and Leung, 2008; Lin et al., 2013; Tran et al., 2013). In this study, the particle sizes of sand in the laboratory tests were scaled up by a factor of 7 for DEM simulations. It should be noted that different researchers adopted different scale factors to ensure enough number of particles in the simulations. There was no agreed value for each study. Ren (2021) performed a series of numerical tests to demonstrate a scale factor of 7 was reasonable. Figure 1 shows the particle size distribution of sand in laboratory tests and DEM simulations. The inset shows a picture of the Fujian Standard sand under a microscope, which reveals that the particles were subrounded. The magnification of the microscope was 30 times the original size. It was also used as a reference to create a general shape of the sand particles in the numerical sample.

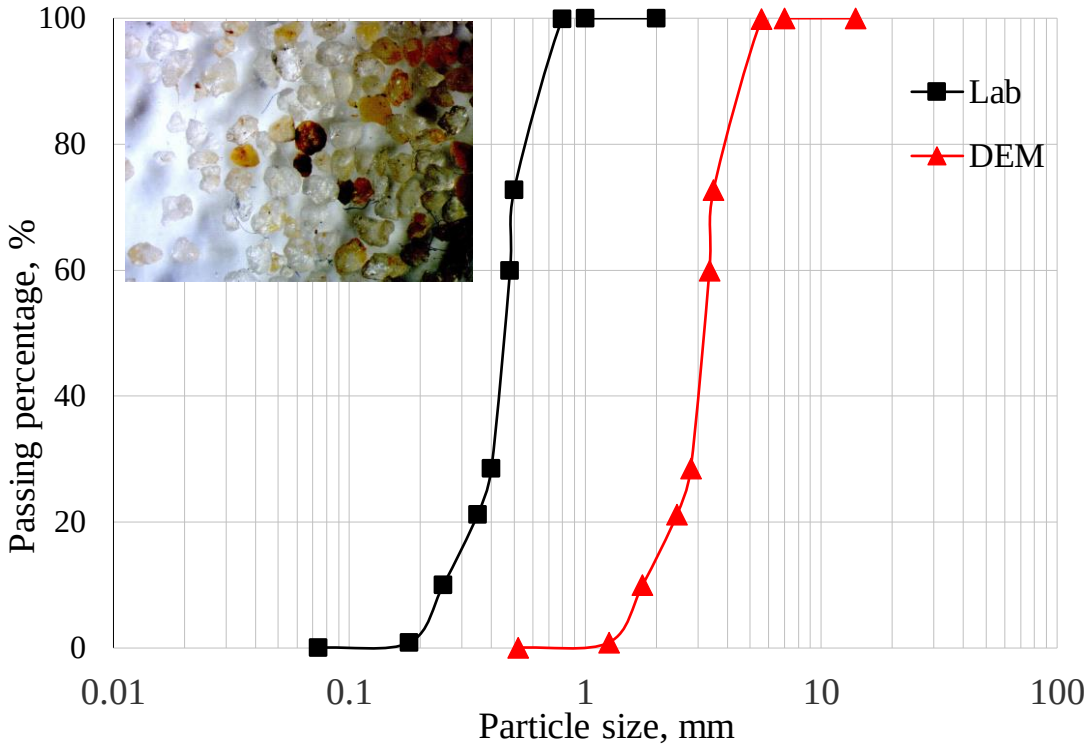

Figure1. Particle size distribution of sand in laboratory tests and DEM simulations

With the help of MorphologI G3 from UCL (Ren, 2021), particle shape factors as shown in Table 1 were calculated. Morphologi G3 is a particle characterization instrument installed with a laser scanning optical microscope that can capture two-dimensional images of the sand grains and then automatically calculate the size and shape factors, such as aspect ratio, circularity and convexity, based on 2D measurements of dimensions, area and perimeter of each particle (Fan et al., 2021). Table 1 presents the measured average value of each shape factor of the sand particles, and the shape factors of the adopted DEM particle clump as shown in Figure 2(a). Efforts were made to ensure that the values of shape factors such as elongation and convexity are similar. Note there were some limitations of these 2D measurements, such as the flatness Index was not calculated, so it was calibrated against experimental results. Figure 2(b) shows the entire sand sample with 15,664 randomly oriented particles generated in the direct shear test box. The numerical simulations were conducted at three different confining stresses, namely 30, 50 and 100 kPa, the same as those in the laboratory shear box tests. A simple contact model of the PFC^{3D} version 5.0 was used (Itasca, 2018). The sand was first generated at the densest

state using an initial friction coefficient of 0.0, and then slowly compressed to the specific normal stresses with the friction coefficient of 0.2. More details on the preparation of experimental direct shear tests and the step-by-step DEM procedure for direct shear tests on sand can be found in Ren (Ren, 2021). The input parameters of DEM investigations were listed in Table 2. It should be noted that the input parameters adopted for the direct shear tests are E^* (sand particle effective modulus) and $k_n^{[S]}/k_s^{[S]}$ (Normal-to-shear stiffness ratio for sand particles). E^* influences the peak shear stress value and $k_n^{[S]}/k_s^{[S]}$ have an obvious effect on the stiffness. During the calibration process, different values for E^* and $k_n^{[S]}/k_s^{[S]}$ were attempted, and then a final set of values E^* = 40 MPa and $k_n^{[S]}/k_s^{[S]}$ = 1.2 were obtained. It can be observed that the shear stresses obtained from DEM modelling agree reasonably well with the experimental results at various normal stresses, as shown in Figure 2(c). This suggests that the numerical model can give good reproduction of the shear behaviour consistent with the corresponding experimental tests.

Table 1. 2D particle shape information obtained from MorphologI G3 and 3D shape information adopted in DEM numerical model

Shape parameter	2D from MorphologI G3	3D for DEM
Elongation index (EI)	0.756	0.75
Circularity	0.928	×
Convexity (Cx)	0.958	0.97
Flatness index (FI)	×	0.81
Roundness (R)	×	0.28

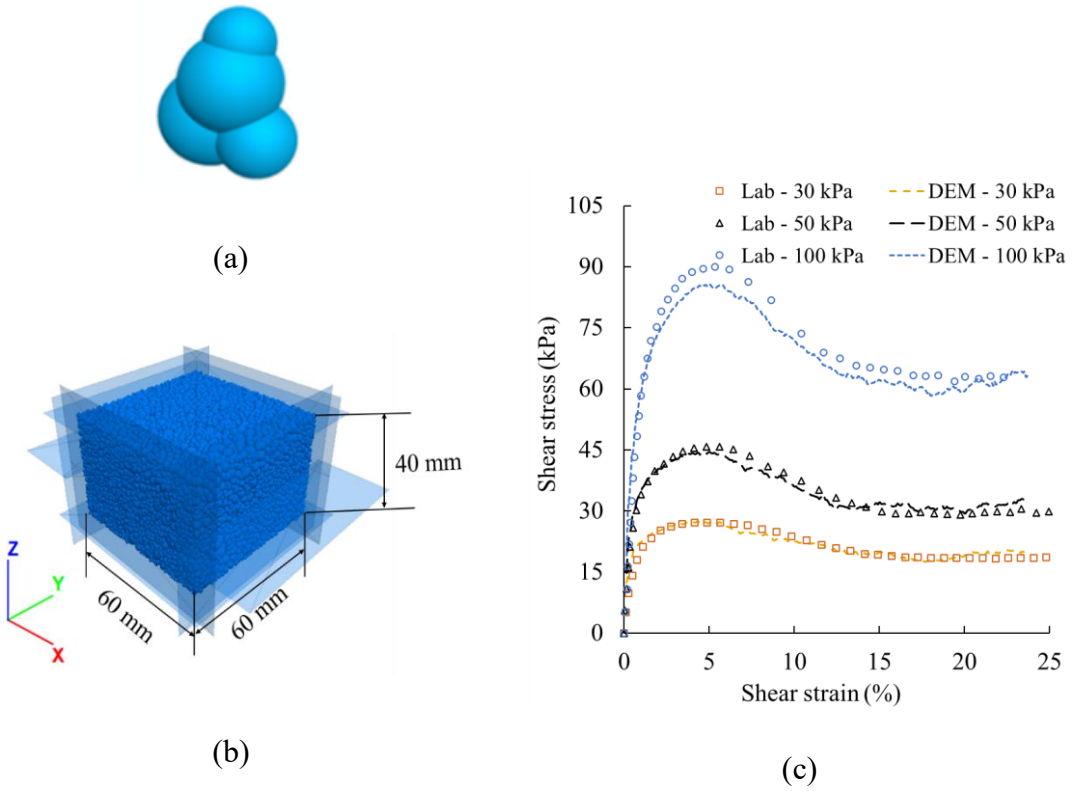

156 **Figure 2. (a) Particle shape adopted in DEM simulation; (b) Initial sample**
157 **preparation in direct shear box; (c) Calibration results of direct shear tests for**
158 **sand**

159 **Table 2. Input parameters for DEM modelling of sand**

Parameter	Sand
Density of the soil particles [kg/m^3]	2650
Sand particle diameter [mm]	Gradation as shown in Fig. 1
Sand particle effective modulus, E^* [MPa]	40
Normal-to-shear stiffness ratio for sand, $k_n^{[S]}/k_s^{[S]}$	1.2
Friction coefficient of the sand particles	0.2
Friction coefficient between the sand particles and the walls	0.0

160 **2.2 Numerical tensile tests**

161 Both laboratory and numerical tensile tests were conducted to obtain the model
162 packing and input parameters for rubber tyres. Three similar tyre strip samples were tested
163 to ensure repeatability. Figure 3(a) shows the relationship between tensile stress and

tensile strain. The tensile strength of the tyre strips is high and around 60-70 MPa. For tensile strain below 20%, there is a linear relationship between tensile stress and tensile strain. From beyond 20% until breakage (at 105% on average), tensile strain exhibits a nonlinear relationship with tensile stress. Considering that most existing tests did not pull the tyres to breakage, we selected model data below a 16% tensile strain from test 1 (Figure3(a)) as a reference for further numerical calibration. In the numerical tensile test, a body-centred cubic (BCC) structure and a simple contact bond model of PFC^{3D} version 5.0 were used to prepare a tyre specimen (Ren et al., 2020). More details on specimen preparation and relevant parametric studies can be referred to Ren (2021). The calibrated numerical tensile stress in Figure 3(b) shows a good agreement with the experimental data. This DEM simulation with the chosen set of parameters satisfactorily models the properties of a rubber tyre in the laboratory tests. The input parameters of DEM investigations were listed in Table 3.

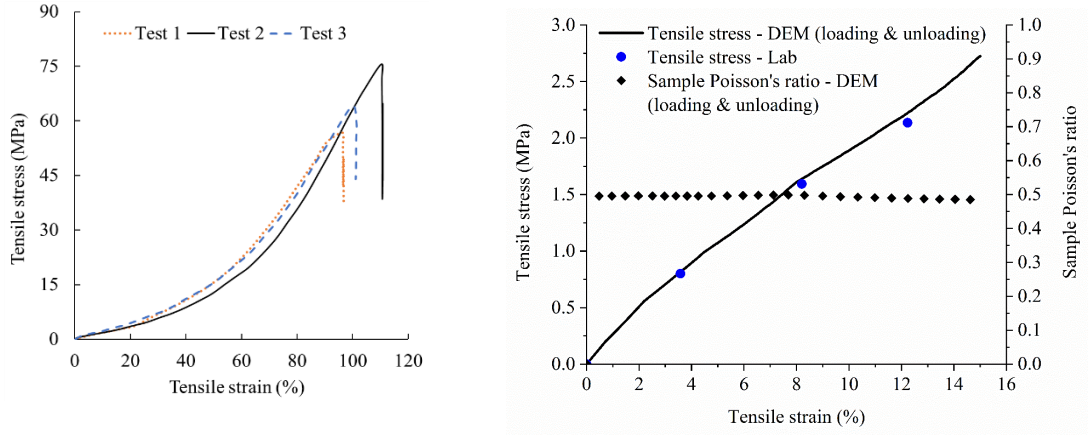

(a) (b)

Figure 3. (a) Tyre strip tensile test results; (b) Comparison between the numerical and the experimental tensile test results

Table 3. Input parameters for DEM modelling of tyre strip

Parameter	Tyre
Density of the tyre particles [kg/m^3]	1100
Particle diameter [mm]	0.5
Coefficient of inter-particle friction [μ]	0.9

Tyre particle effective modulus, E^* [MPa]	20
Normal-to-shear stiffness ratio for tyre, $k_n^{[T]}/k_s^{[T]}$	4.5
Tensile strength, *cb_tenf* [N]	2e150
Shear strength, *cb_shearf* [N]	2e150
Friction coefficient of the tyre particles	0.7

2.3 Numerical tyre - soil interface direct shear tests

Simulations of the interface direct shear test shown in Figure 4(a) were conducted under three normal stress conditions (30 kPa, 50 kPa and 100 kPa), the same as those in the laboratory tests (conducted by Ren (2021). The sand samples were sheared at a displacement rate of 1 mm/s to a total displacement of 10 mm. The corresponding numerical interface tests simulation procedure was introduced by Ren (Ren, 2021). It should be noted that the set of parameters for sand was from the calibration results in Table 2, and the set of parameters for the tyre strip was from the calibration results in Table 3. In this section, only the friction coefficient between the tyre strip and sand particles needed to be calibrated. By trial and error, the friction coefficient between rubber tyre strip and sand particles was determined as 0.7. A comparison between the numerical and the tyre-sand interface experimental results were illustrated in Figure 4(b), showing a good match between the experimental results and the simulated data.

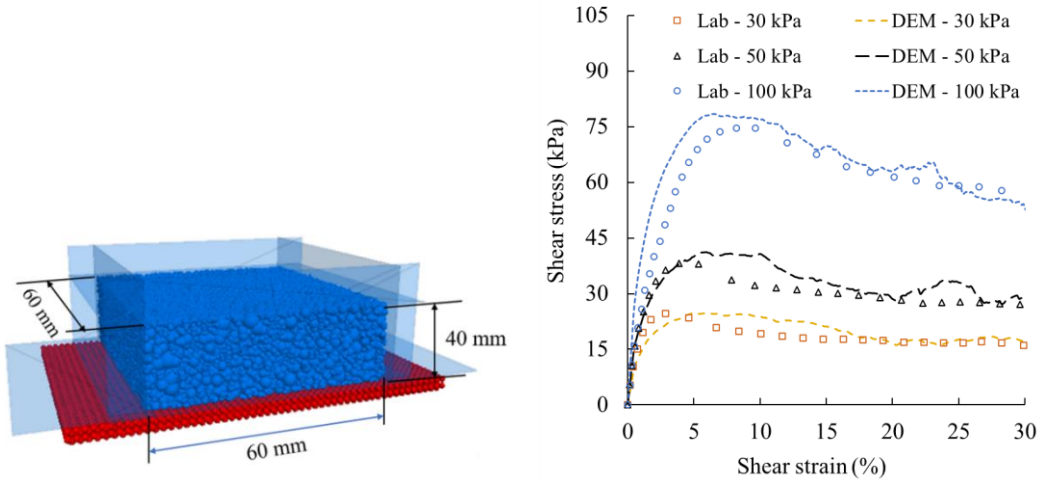

（a） （b）

Figure 4. (a) DEM model for the tyre strip-sand interface direct shear test; (b)

197 **Calibration results**

198 **2.4 Numerical tyre - soil pull-out tests**

199 To obtain valuable insights into the reinforcement mechanism of tyre-reinforced soil,
200 this section presents rubber tyre strip-soil pull-out tests both experimentally and
201 numerically. The laboratory tyre reinforced soil pull-out tests were conducted by Li et al.
202 (2017). In the rubber tyre and sand pull-out tests, the physical properties and the particle
203 size distribution of Fujian Standard Sand were introduced in section 2.1. The relative sand
204 density achieved during sample preparation in pull-out tests was 0.95. Three similar tyre
205 strips were laid on a 20-mm thick layer of compacted sand in each test. The ends of the
206 tyre strips located outside the box were attached to the pull-out clamp as shown in Figure
207 5(a) and Figure 5(b). The tyre strips inside the shear box were 420 mm in length, 30 mm
208 in width, and 15 mm in height. Figure 5(c) shows the results of the pull-out tests, peak force
209 increased as the normal stress increased for tyre strips. Here, the pull-out force was
210 normalized by the width of the box (i.e., 300 mm) for comparison. The differences in
211 stiffness tend to decrease as the normal stresses increase. More details about the
212 displacement, pull-out speed and pull-out force can be found in Li et al. (2017).

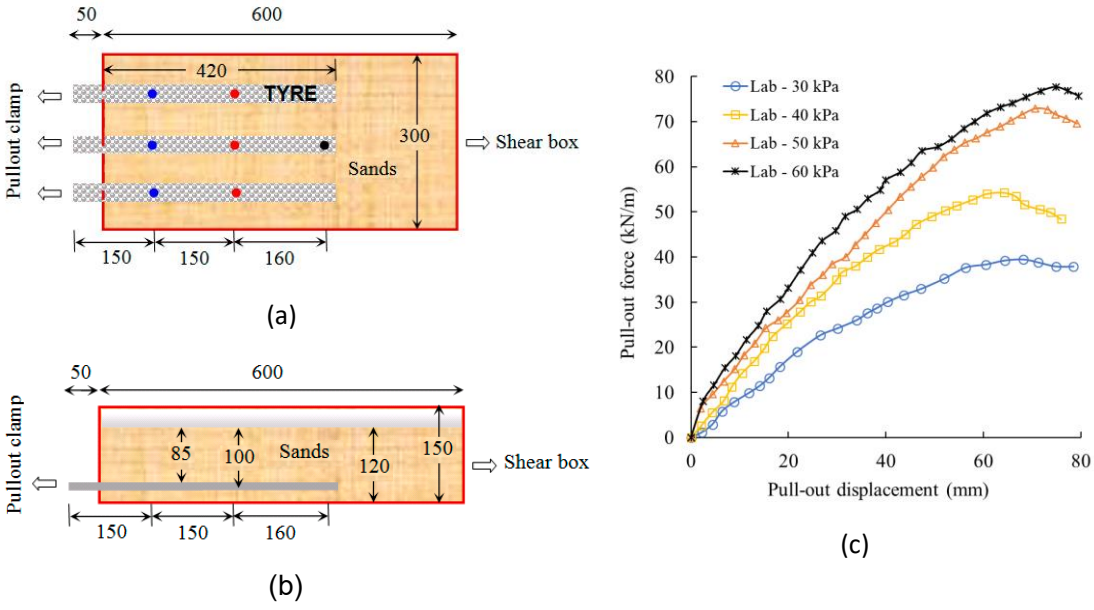

213 **Figure 5. (a) Pull-out tests of tyre strips reinforced sands: plan view; (b) elevation**
214 **view; (c) pull-out force-displacement curves under various stresses (after Li et al.,**

215 **2017)**

216 In the numerical pull-out tests, considering computational power, dimensions for both
217 pull-out box and tyre strip were downscaled relative to those in the laboratory tests. The
218 box dimensions in numerical simulations were 60 mm in length, 50 mm in width and 40
219 mm in height. The height and width were designed by minimising the boundary effect, and
220 the length of the box was intentionally shortened. One tyre strip was adopted in the pull-
221 out test. The dimensions of the rubber tyre specimen were 60 mm in length (the length
222 inside the sand specimen was 50 mm, the length outside the box for clamping was 10 mm),
223 10 mm in width and 3 mm in height. The sand particles and rubber tyre were created
224 following the same procedure described. All micro input parameters for DEM pull-out test
225 simulations were listed in Table 2 and Table 3. The basic DEM sample preparation
226 procedures of pull-out tests generally have three stages: (1) create walls and prepare sand
227 - tyre specimens, (2) create and consolidate the sand specimen to the desired confining
228 stress level and (3) execute the pull-out process. Note the size of the opening where the
229 tyre left the box was constantly adjusted numerically following the deformation of the tyre
230 strip.

231 Figure 6 shows the embedded rubber tyre in the pull-out tests. The particle size of
232 the rubber tyre specimen was 0.5 mm, while the mean size (D_{50}) of the sand particles was
233 3.36 mm, having been scaled up by a factor of 7 for DEM simulations in this study. Even
234 the minimum sand particle size was 0.518 mm after scaling up. This means that
235 interlocking between sand particles and rubber tyres was minimized during the pull-out
236 process. The pull-out process was executed with a specified constant velocity of 0.25 m/s
237 at the clamp end. The external 10mm (blue particles) of the tyre strip were ‘clamped’ and
238 pulled leftward together horizontally under the same velocity. To minimize the dynamic
239 effects, the pull-out rate was gradually increased linearly over time from zero to the final
240 rate. The pull-out process terminated when the clamp end displacement exceeded 10 mm.
241 During the simulation, the displacements and force at the clamp end along the pull-out
242 direction (i.e., the negative direction along the x-axis as shown in Figure 6) were monitored
243 during the pull-out process. Here, the pull-out force was calculated by summing all the ball-

clump contact forces in the x-direction. Following these procedures, three numerical pull-out tests were conducted. The corresponding target stress levels were 30 kPa, 50 kPa and 100 kPa, respectively. More details can be found in Ren (Ren, 2021).

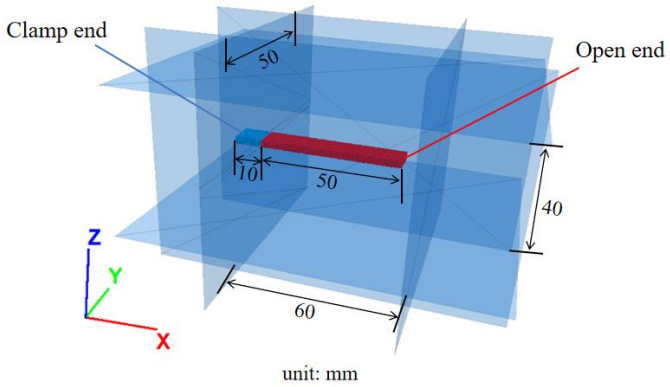

Figure 6. Clamp settings for the DEM model of a tyre strip pull-out test

3. PULL-OUT BEHAVIOUR OF TYRE STRIP EMBEDDED IN SOIL

3.1 Macro responses during the pull-out process

Figure 7(a) shows the development of pull-out force against clamp end displacement. A comparison between extensible and inextensible tyre strips (without tyre extension) was also presented in this figure. Here, the extensible tyre strip cases represent the calibrated tyre strips with a Poisson's ratio of 0.5. The pull-out process was executed with a specified constant velocity of 0.25 m/s at the 10 mm clamp end, whereas extension and deformation were allowed for the rest of 50 mm of the tyre strip. The inextensible tyre strip cases strictly exclude tyre extensions, the corresponding pull-out process was executed on the entire tyre specimen rather than just at the clamp end. It was observed that for extensible tyre strip cases, the pull-out forces at different normal stresses increase approximately continuously and then stay at the peak pull-out forces without strain-softening as pull-out displacement increases from 0 mm up to 10 mm. A general observation is that the peak pull-out force increases with a rise in normal stress.

The results also indicate that higher normal stress can extend the critical pull-out displacement corresponding to the peak pull-out force. Overall, although the values for pull-out forces in numerical simulations are quite small as shown in Figure 7(a), these

general trends are consistent with the experimental findings reported by Li et al. (Li et al.,2017) shown in Figure 5(c). It is believed that a shortened pull-out box and reduced rubber tyre specimen dimensions (Length ratio = 420/50 = 8.4) with the use of a single strip of a rubber tyre in the simulation all potentially decrease the reinforcement ability of the specimen during the pull-out process. For example, the experimental peak pull-out resistance under normal stress of 30 kPa is around 35 kN/m, as shown in Figure 5(c). The experimental pull-out resistance of a single shorter tyre strip embedded in a box with a width of 50mm could be approximated to be 35 /3 /8.4*50 = 69.4N. The result matches the magnitude for a simulated pull-out force of around 66.6 N at a peak state under 30 kPa, as seen in Figure 7(a). It should be noted that the pull-out force in the experimental test results plotted by Li et al. (2017) was measured in kN/m and it was normalized by the width of the box for comparison. Some interaction between neighbouring tyre strips may affect the result, hence the pull-out force may not be simply divided by a factor of three, and the exact effect of tyre length will be presented later in this paper. In addition, the experimental tyre strips have irregularities, such as the natural curvature of the tyre and the grooves on the tyre surface, the corresponding simulations should be recreated according to the real shapes of the tyre strips in theory to replicate the exact tyre strip pull-out behaviour. Overall, the scaled pull-out force was considered comparable with the corresponding experimental results.

Comparing extensible and inextensible tyre strip cases, the results show that the pull-out forces of the inextensible tyre strips increase much faster than that of the extensible tyre strips and approach the peaks at lower critical pull-out displacements. In contrast, the pull-out force-displacement curves of the extensible tyre strips follow a comparatively slower rate and reach the corresponding peak at a higher critical pull-out displacement. All curves show an initially higher constant tangent stiffness, then followed by gradually decreasing stiffness until the peaks. The results also show that the peak pull-out forces are similar for both the extensible and the inextensible tyre strip cases under each normal stress level. This is because the extensible tyre strips are more elastic and hence extend longer to reach the same pull-out load compared to the corresponding inextensible tyre strip cases. It appears that the sawtooth undulation in the 100 kPa simulations (in Figure

7(a)) is more significant. This is possibly induced by a pressure-dependent numerical inaccuracy and is related to the pull-out rate. During the pull-out process at a higher pressure, the particle contact force chains columns sustain more easily within the shear band. As pull-out force continues to increase, particle contact forces cannot redistribute in time. It is until finally, slipping occurs at contacts and columns buckle, then particle contact forces redistribute and the pull-out force then reduces. We can also explain the phenomenon using the inertial number. To keep the inertial number the same, a higher confining pressure implies that a lower loading strain rate is required. Some simulation trials were performed. Results indicate that if a simulation was performed at a slightly slower pull-out velocity, the force fluctuation reduces although the average pull-out force remains the same.

Figure 7(b) presents the evolution of the vertical displacement of the DEM sand sample during the pull-out process at different confining pressure. The sample experienced slight contraction during its initial pull-out (about 1~2 mm) before dilation. Displacement at the peak pull-out force associates well with the maximum dilation rate. Higher confining pressure suppresses the dilation of sand, hence resulting in a smaller total vertical displacement. Like the peak pull-out forces, the maximum dilation rate occurs at a higher critical pull-out displacement when confining pressure increases. So it can be anticipated that the final vertical displacement also happens at a higher pull-out displacement than 10 mm when confining pressure is high at 100 kPa. This might imply that the specific peak pull-out force (shown in Figure 7(a)) can still increase beyond 10 mm. Under high confining stress, vertical dilative particle movements are restricted, hence requiring a longer pull-out displacement to reach the peak pull-out force. Related to this, longer tyre strips provide more space allowing more sand particles to interlock and buckle more uniformly along the interface, thus helping obtain a fully-developed progressive failure. More discussions will be made later. Figure 7(b) also shows that the vertical displacements and the dilation rate of the inextensible tyre strip cases are always larger than that of the extensible cases. However, the final vertical displacements of extensible and inextensible cases reach a similar level. This can be seen clearly from the 30 kPa and 50 kPa cases, but not the 100 kPa cases.

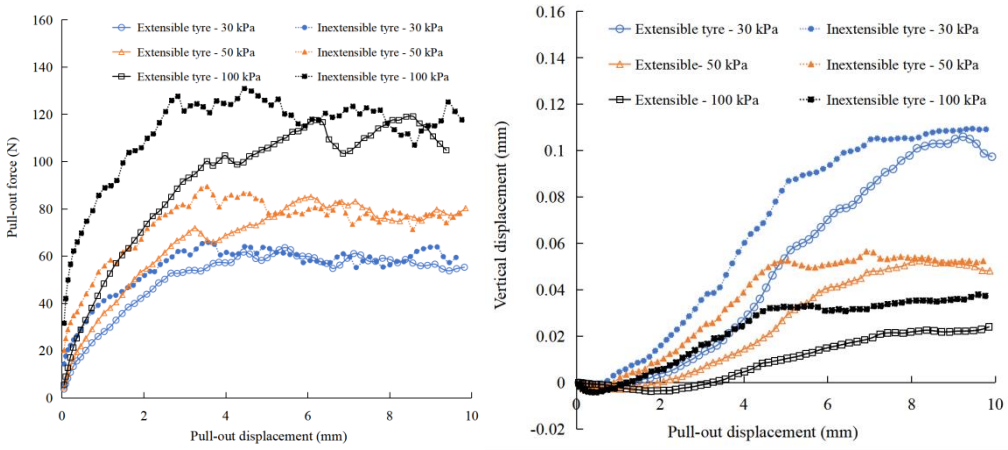

(a) (b)

Figure 7. (a) Pull-out test results from extensible and inextensible tyres: pull-out force; (b) vertical displacement

3.2 Interface shear force distribution along the tyre strip

To gain further detailed insights into the mechanism of tyre strip-sand interaction under pull-out loads, some micro-scale observations were provided, including the contact shear force distribution along the tyre strip, accumulative sectional interface shear forces along the tyre strip, and also particle displacement, particle velocity vectors, particle spin and orientation of the particle contact force of the sand particles around the tyre strip. Taking the case with 30 kPa normal stress as an example, the micro-mechanical data was analysed at three representative states: initial, at peak and final 10 mm pull-out state. Figure 8(a) illustrates the locations of the five sections along the tyre strip–sand interface, measured from the left side wall of the pull-out box. The magnitude of the x-direction contact forces between the tyre and the sand particles were calculated within each section and then summed up to obtain the total pull-out forces of the tyre strip. Figure 8(b) shows the accumulation of pull-out force at the three different states: initial 2.0-mm pull-out state, peak 5.4-mm pull-out state, and final 10-mm pull-out state of the extensible tyre strip under normal stress σ_v of 30 kPa.

It is evident from Figure 8(b) that the increase of accumulated pull-out forces is slow in section 1, then faster in region 2 ~ 3, and then slow again in section 4 ~ 5. This implies that pull-out forces in the middle portion of the tyre strip are much higher than the pull-out forces at the two ends of the tyre strip. These different values of sectional interface shear

forces along the tyre strip imply that each part of the tyre strip was mobilising a different frictional resistance. Assuming the vertical stress acting on each section is similar in magnitude, shear failure should occur first in the middle portion of the tyre strip, indicating a progressive failure. Progressive failure was also observed by Li et al. (2017), who performed laboratory pull-out tests on sand reinforced with long rubber strips.

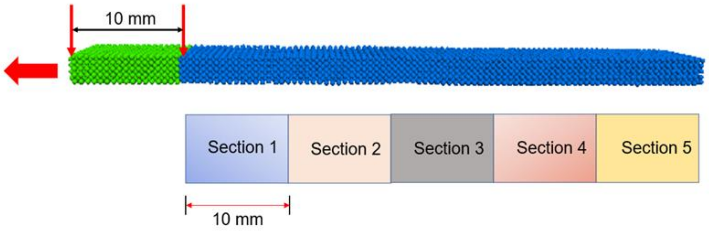

(a)

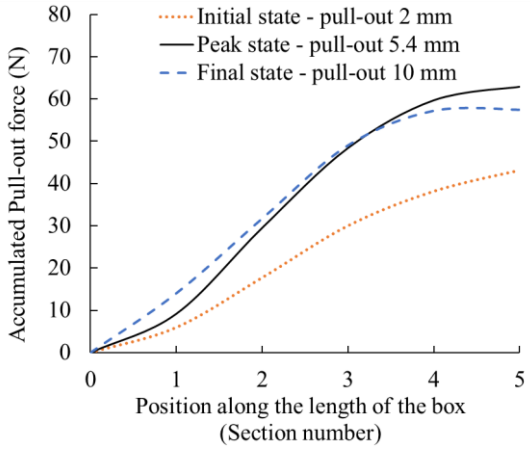

(b)

Figure 8. (a) Illustration of 5 sections along the pull-out box; (b) Accumulated pull-out force along the extensible tyre strip at three different states (σ_v = 30 kPa)

Figure 9 shows the distribution of sand particle displacement at the three different pull-out states. Figure 9(a) shows the movement zone of the sand clump particles forming an arch around the rubber tyre at an initial pull-out of 2 mm. The area with sand particles movement is higher near the middle zone of the tyre strip than those near the two ends of the tyre strip. Figure 9(b) shows the movement zone becomes bigger and extends closer to the left wall at a peak pull-out of 5.4 mm. The height of the sand particles' movement zone increases from the clamp end (left wall) to a maximum value in the middle, then decreases again towards the open end. This peak state should correspond to the moment when the shear band is fully developed. This means that the rubber tyre elements reach a shear failure strength first in the middle section and then extend towards the pull-out clamp

end before finally reaching the open end. It can also be seen that the thickness of the particle movement zone below the tyre is smaller than that above the tyre strip. The overall shear band thickness is around 7 times D_{50} (3.36mm) of the DEM clump. The distance between the tyre strips and the bottom boundary of the experimental apparatus was 20mm, which is about 42 times D_{50} (0.48mm) of Fujian sand, therefore there should be a minimum boundary effect in the experimental result. Figure 9(c) shows the particles' movement zone at the final pull-out of 10 mm. The shape of the zone is similar but slightly bigger and the height is even higher at the clump end. Note here at the final state, the open end of the tyre strip has moved, implying a full failure of the tyre strip has occurred. This left a relatively loosely packed zone behind the tyre strip. Tensile strains of tyre strips during the pull-out process were also calculated based on the recorded displacement response of tyre strips. The tensile strain of the extensible tyre strip at the initial pull-out state, peak state and the final pull-out state was 1.47%, 2.30% and 2.44%, respectively, whereas that of the inextensible tyre strip had zero tensile strain at each state.

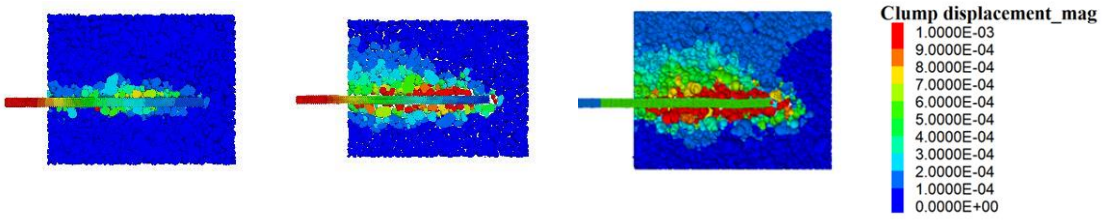

Figure 9. (a) Particle displacement field of an extensible tyre during a pull-out test (σ_v = 30 kPa) at the initial pull-out 2 mm; (b) at the peak pull-out 5.4 mm; (c) at the final pull-out 10 mm.

3.3 Contribution of sectional interface shear force to total pull-out force

Figure 10 summarises the quantitative contribution of interface shear forces from each section of the tyre strip to the total pull-out force at the three states. Figure 10(a) shows the state of pull-out 2 mm for an extensible tyre. The contributions of interface shear forces from section 2 (27%) and section 3 (28%) are noticeably greater than those of the right-side sections, namely section 4 (19%) and section 5 (11%). Figure 10(b) shows that the interface shear forces at the peak state follow a similar trend but even higher percentage

contribution from the middle sections. The contributions of interface shear forces from section 2 (32%) and section 3 (30%) are noticeably greater than those of right-hand sections, namely section 4 (18%) and section 5 (5%) for the rubber tyre. Comparing the peak 5.4 mm state to the 2 mm state, although the percentage contribution of section 5 is smaller, the absolute magnitude of sectional interface shear force is similar to around 3~4 N. Note the movement of the sand particles is also the highest in regions 2~3 (Figure 9), hence inducing the highest interface shearing force in this region. This also implies that there is a more extensive shear banding zone and interlocking mechanism (i.e., more relative movement/ dilative shearing between the tyre and the sand particles) at work between the rubber tyre and sand particles in the middle portion of the tyre strip. Figure 10(c) shows the force distribution along the tyre strip for the final state with 10 mm pull-out displacement. Much percentage contribution of section 1 increases from 14% to 24%. The principal pull-out forces are from sections 1, 2 and 3, which provide contributions of 24%, 31% and 30% to the total pull-out force, respectively. At this stage, global failure had happened due to the tyre detaching from the sand, which was explained in Figure 8. The total pull-out force remains similar compared to the peak state. The percentage contributions of sections 2 and 3 remain similar. But the percentage contribution of section 1 increases whereas that of sections 4 and 5 reduces. The low percentage contribution in section five is probably because the tyre has moved away from this section due to global failure. Figure 10(d)-(f) reinforces that similar progressive failure also occurs in the inextensible tyre stirps, although the peak state occurs earlier at 3.5 mm pull-out. The shift of the location of the highest percentage contribution from the middle section to the clump end section is even more obvious.

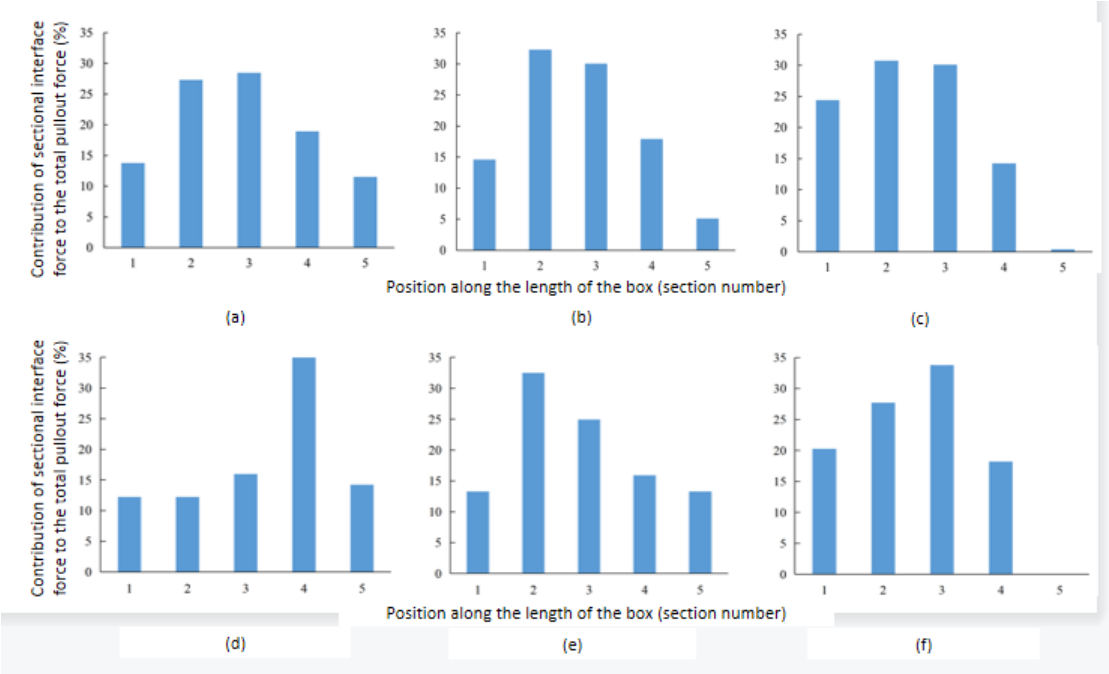

Figure 10. (a) Contribution of sectional interface force to the total pull-out force during pull-out test (σ_v = 30 kPa) for inextensible tyre at initial state; (b) inextensible tyre at peak state; (c) inextensible tyre at final state;(d) extensible tyre at initial state; (e) extensible tyre at peak state; (f) extensible tyre at final state

Figure 11(a) shows the contact forces network within the specimen at the peak state. Zone 2~3 gives the largest dilation. The space at the peak state indicates that a gap of the loosely packed particles has already started to form behind the tyre strip. It should be noted that the tensile strain of rubber tyre was around 2.30% at this state. Approximately 5mm of movement at the clamp end and approximately 3mm movement at the open end were observed. The difference should attribute to the extensibility of the tyre strip, which is 2.3%, i.e., 1.15mm. To better understand the development of the force chains, the contact and force distributions can be visualized with polar histograms. Ouadfel and Rothenburg (2001) proved that the evolution of normal contact force [f_n] plays the most significant role in determining the overall shear strength of granular materials. On the other hand, Rothenburg and Bathurst (1989) proposed that the complicated tensor that describes anisotropy features of [f_n] in granular assembly can be simplified using the second-order Fourier series approximation, i.e.:

$$f_n(\theta) = f_0[1+a_n\cos 2(\theta - \theta_n)] \quad (1)$$

where f_0 is a constant equal to the average normal contact force; a_n and θ_n are the fitting parameters that stand for the magnitude of the directional variation and the principal direction of anisotropy, respectively. θ is the direction of the normal force obtained by statistics. Figure 11(b)~(d) presents the anisotropy features of normal contact forces in 3 typical regions projected onto the x-z plane (side view). The area enclosed by each 10-degree interval of the polar histogram represents the magnitude of the total normal contact force normalized by the average normal contact force over all contacts and by the total number of contacts. Under the peak state, the values of average contact normal force f_0 at the peak state were 10.6 N, 11.3 N and 7.9 N for sections 1, 2 and 4 respectively. The value of f_0 in section 2 is larger than that in section 1 and section 4. Overall, the anisotropic principal direction develops and rotates from approximately probably from a vertically orientated direction (section 4) to an apparent horizontally oriented direction (section 1) when the interface shear force develops. In section 2, there is the most significant rotation to the principal stress direction. These observations illustrate that the positional rearrangement of particles allows the reinforced system to effectively resist external loads (pull-out load and normal pressure).

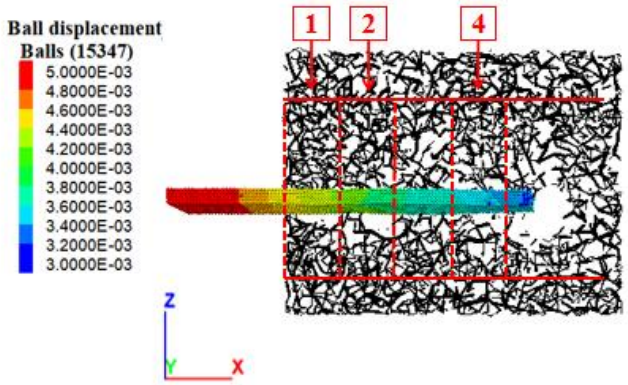

(a)

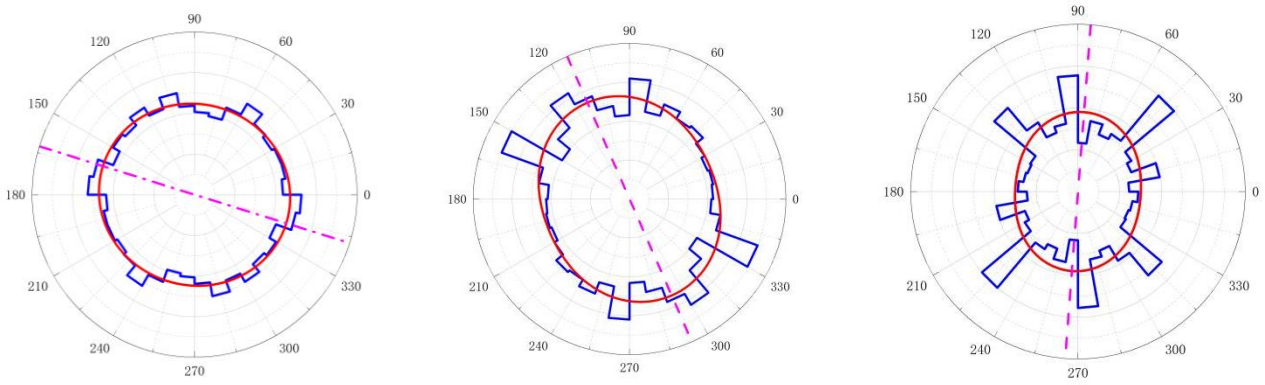

(b) (c) (d)

Figure11. (a) Region of interest at peak state under 30 kPa; (b) evolution and anisotropy of normal contact force at peak state in section 1; (c) peak state:section 2; (d) peak state: section 4

3.4 Velocity vectors and particle spin of sand particles surrounding the tyre strip

Figure 12(a) ~ (c) shows the velocity vectors of sand particles at the three states (initial state, peak state, and final state) during the pull-out tests. It should be noted that velocity vectors were all drawn at the same scale. These figures display the mobilisation of sand particles along the rubber tyre strip during the pull-out process. In the case of horizontal pull-out to the left for the rubber tyre strip, the sand particles surrounding the rubber tyre move together with the rubber tyre strip. The interface friction between the rubber tyre strip and sand resists movement, which causes slight orientation changes in the velocity vectors (from vertical to diagonal), as shown in Figure 11. Furthermore, the dilative zone for sand particles surrounding the rubber tyre strip is larger for the peak state than in the other two states. This is also consistent with the results under 30 kPa normal stress shown in Figure 7.

Figure 12(d) ~ (f) shows the particle spin of sand particles surrounding the rubber tyre strip at the three states (initial state, peak state, and final state) during the pull-out tests. The particle spin represents the clump angular velocity, which was obtained automatically from the software. It should be noted that particle spins were all drawn at the same scale. These figures supply additional information regarding sand particle movement during the pull-out tests. More particle spins appear at the peak state, as shown in Figure 12(e), which is consistent with Figure 12(b). In addition, the particle spins below and above the rubber

tyre strip are nearly symmetrical. Although the pictures only show a particular 2D section of the 3D simulation, it is typical that the shear banding zone is around 10 particles in diameter.

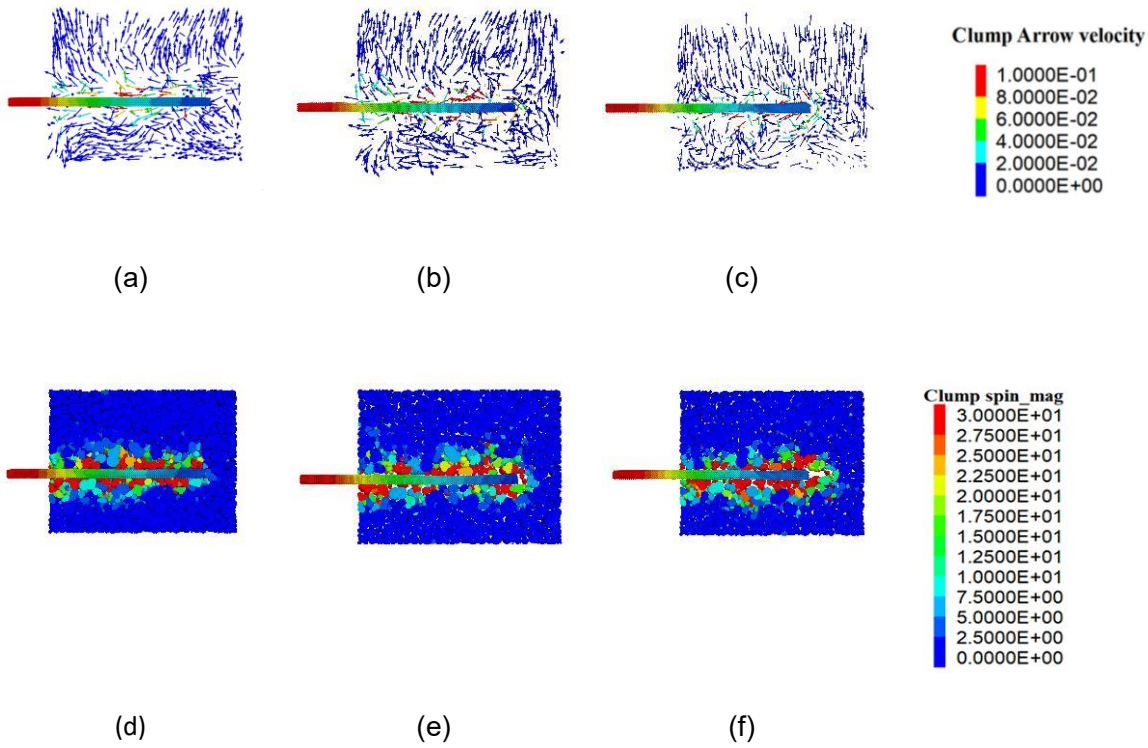

Figure 12. (a) Particle velocity field at initial state; (b) particle velocity field at peak state; (c) particle velocity field at final state; (d) particle rotation at initial state; (e) particle rotation at peak state; (f) particle rotation at the final state

3.5 Influence of tyre strip length on pull-out test results

Given that the length of the rubber tyre strip in the laboratory pull-out test (Li et al., 2017) was 420 mm, exploring the rubber tyre length effect on pull-out test results could be meaningful. This subsection presents some macro-scale and micro-scale data from the parametric studies on the rubber tyre length effect. For the numerical pull-out tests, the box was 120 mm long, 50 mm wide, and 40 mm high. The pull-out displacement was 20 mm. Lengths 50 mm, 75 mm and 100 mm were selected for the rubber tyre to perform the numerical pull-out tests under 30 kPa normal stress. Figure 13 shows the development of the pull-out force against the clamp end displacement. The rubber tyre length seems to

have little effect on the initial stiffness of the curves during the initial pull-out displacement, probably due to the absence of significant particle movement at this state. However, with further pull-out displacement, the peak pull-out force shows an obvious nonlinear increase as rubber tyre length increases. The peak pull-out force happens as soon as it deviates from the initial curve, the locations are indicated by the circle marks, and the pull-out forces are linearly proportional to the tyre length, as shown in the sub-figure. Note this linear proportional relationship may not be valid if the tensile strain of the tyre strip is beyond the range of this study. This finding could potentially be beneficial to practical design, as it is possible to calculate the exact pull-out force and design for the spacing of a series of long tyre strips for use in a retaining wall. Fox and Kim (2008) also observed that specimen length has significant effects on the measured shear strength when analyzing the progressive failure at the geomembrane/geosynthetic clay (GCL) liner interface using a large direct shear box.

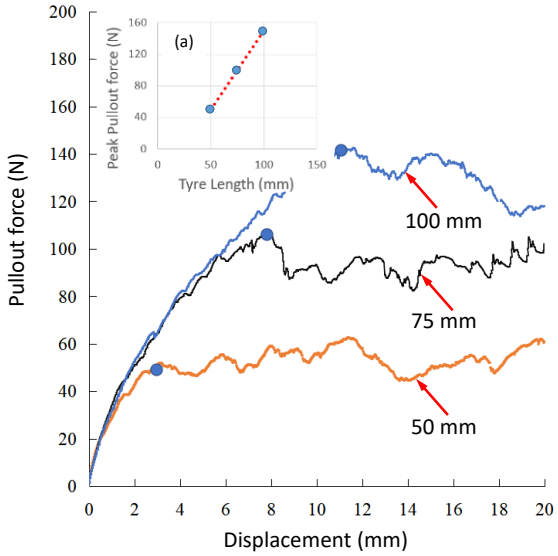

Figure 13. Effect of tyre strip length on pull-out tests results

Figure 14 summarises the quantitative contribution of interface shear forces from each section of the tyre strip to the total pull-out force at the three states. Compared to the shorter 50 mm tyre strip (as shown in Figure 10), the rate of change of sectional contribution appears to be less significantly different. A longer tyre strip seems to be able to spread the interface frictional resistance and interlocking shear forces more evenly distributed along the tyre strip. That means longer tyre strips expand the action range of

519 tyre strip-sand interactions, thus achieving a better reinforcing effect. Figure 14 reveals two
520 distinctive zones of high percentage sectional interface shear forces in section 3~4 and
521 section 6~7 at the peak state as shown in Figure 14(b). Then, these zones shift forward
522 towards the clump end to sections 2~3 and 5~7 at the final state as shown in Figure 14(c).

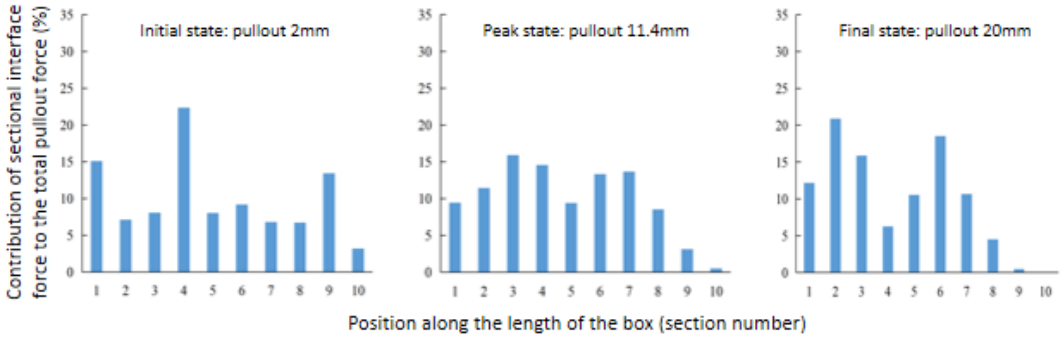

523

524 (a) (b) (c)

525 **Figure 14. (a) Contribution of sectional interface shear force to the total pull-out**
526 **force during a pull-out test for an extensible tyre at initial state; (b) extensible tyre**
527 **at peak state; (c) extensible tyre at final state (the tyre length inside the sand**
528 **specimen was 100 mm)**

529 To illustrate this phenomenon better, Figure 15 shows the velocity vectors of the sand
530 particles at the final pull-out state, and the influencing zone that constitutes the dilative
531 zones affects the final peak pull-out force. The particle clumps velocity vectors reveal the
532 directions of particle movements. There are circular motions of particles near the interface.
533 When the rubber tyre length is 50 mm, there is only one circulation motion along the rubber
534 tyre. For a rubber tyre length of 75 mm with a longer influencing zone, the velocity vectors
535 appear to create more than one circulation, possibly two. With a rubber tyre length of 100
536 mm, the influencing zone around the rubber tyre develops a more homogenous distribution,
537 unlike the turbine distribution in the other two cases. The reason may be that the longer
538 rubber tyre can provide more space allowing more sand particles to allow the shear band
539 to form uniformly along the interface during pull-out.

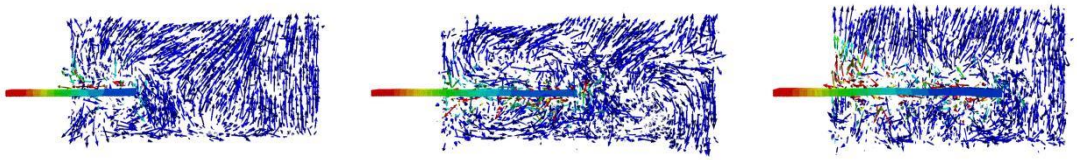

(a) (b) (c)

Figure 15. (a) Particle velocity field at the final stage of pull-out tests (tyre length 50 mm) ; (b) tyre length 75 mm; (c) tyre length 100 mm

4. CONCLUSIONS

This study investigated the pull-out behaviour of tyre strips embedded in dense granular soil using the three-dimensional discrete element method (DEM) of Particle Flow Code (PFC) version 5.0. The experimental direct shear tests of the sand, tyre strip tensile tests, and tyre strip-sand interface direct shear tests were conducted by Ren (2021) to calibrate the model parameters of sand and tyre strip in terms of their stress-strain relationship, tensile stiffness, and interface shear strength. The calibration results indicate that the present modelling method and the adopted input parameters are reasonable. The interactions behaviour of the pull-out tests was investigated numerically using a simplified small-scaled pull-out box consisting of one piece of tyre strip. The influences of the elastic extension of the tyre and the tyre strip length were explored. The scaled pull-out load was found to quantitatively match the experimental results obtained by Li et al. (2017). Detailed insights into the tyre strip-soil interaction have been explored at the microscopic scale using data such as particle displacement, particle rotation, particle velocity and orientation of contact normal forces etc. during the pull-out process. Some major conclusions can be drawn as follows:

(1) Systematic development of a 3D DEM model for the tyre strip-soil pull-out tests along with corresponding calibration work was presented by comparing results of laboratory element tests and numerical simulations. The results indicate that this is a valid practical tool for investigating the micro-mechanical interactions between tyre strips and sand.

(2) The pull-out force of the tyre strip embedded in dense sand increases nonlinearly with pull-out displacement until the peak state without strain softening. The tyre strip-

reinforced soil exhibits a progressive failure, where each portion of the tyre strip mobilises a different level of shear stress until its sectional peak shear strength reaches a specific distance.

(3) The major contribution of interface shear forces to the macro pull-out force was from the middle segment of the tyre strip sample, where significant particle movement was observed. Induced anisotropy can be revealed by the rotation of principal contact force direction and the displacement of particles. Particles in the middle segment rearrange and rotate from the original microstructure to a relatively stable inclined anisotropic microstructure during shear mobilisation. These micromechanical processes govern the increase of the sectional interface stresses and control the macro-mechanical performance of the tyre strip-reinforced system.

(4) Results of the inextensible tyre strips (extension prohibited) show that the peak pull-out forces are reached faster and with higher initial stiffnesses during the pull-out process than those of the extensible tyre strip cases. As a result, the critical pull-out displacements when peak forces are reached become smaller. This is due to the faster development of the progressive failure along the tyre strip. But the peak pull-out force remains the same as that of the extensible tyre strip under each confining pressure. These suggest that the elastic extensible tyre strips maintain the ultimate safety by having the same pull-out load, but it deforms more flexibly when reinforcing soils which is beneficial to dynamic applications.

(5) Reinforcing soil with longer tyre strips greatly improves pull-out resistance, thus a better reinforcing effect. The peak pull-out force is linearly proportional to tyre length, although tyre length doesn't affect the initial stiffness of the pull-out force-displacement curves. With a longer rubber tyre strip, the shear band zone is formed more uniformly along the sand-tyre interface, as a more homogenous distribution of particle movement can be developed when the tyre strip is longer. For design purposes, it is possible to design for the actual pull-out force and the spacing of a series of long tyre strips for use in a retaining wall based on the finding in this study that the ultimate pull-out resistance is proportional to the length of a tyre strip.

ACKNOWLEDGMENTS

The authors would like to thank the Ministry of Education of China and University College London (UCL) for their generous financial support (Grant no. 201508420167) and the scholarship for PhD study. The first author would also like to express gratitude to the University of Cambridge for providing an opportunity to study at Cambridge Centre for Smart Infrastructure and Construction (CSIC) research group.

NOTATION

Basic SI units are shown in parentheses.

E	sample young's modulus
E^*	particle effective modulus
μ	coefficient of inter-particle friction
$k_n^{[S]}/k_s^{[S]}$	normal-to-shear stiffness ratio for sand particles
cb_tenf	contact bond tensile strength
cb_shearf	contact bond shear strength
σ_v	normal stress

ABBREVIATIONS

ASTM:	American society for testing and materials
BCC:	Body-centred-cubic packing
C_x	Convexity
EI	Elongation index
FI	Flatness index
FSA:	Fourier series approximation
PFC:	Particle Flow Code
R	Roundness
3D DEM:	Three-dimensional discrete element method

REFERENCES

Asadi, M., Thoeni, K., & Mahboubi, A. (2018). An experimental and numerical study on the compressive behaviour of sand-rubber particle mixtures. Computers and Geotechnics, 104, 185-195.

ASTMD6270-98. (2008). Standard practice for use of scrap tires in civil engineering applications-ASTM D 6270-98 (reapproved in 2008).

Bali Reddy, S., Pradeep Kumar, D., & Murali Krishna, A. (2016). Evaluation of the optimum mixing ratio of a sand-tire chips mixture for geoengineering applications. Journal of Materials in Civil Engineering, 28(2), 06015007.

632 Balunaini, U., Yoon, S., Prezzi, M., & Salgado, R. (2014). Pullout response of uniaxial geogrid in tire shred–
633 sand mixtures. Geotechnical and Geological Engineering, 32(2), 505-523.
634 Bosscher, P. J., Edil, T. B., & Eldin, N. N. (1992). Construction and performance of a shredded waste tire test
635 embankment. Transportation Research Record, (1345).
636 Bosscher, P. J., Edil, T. B., & Kuraoka, S. (1997). Design of highway embankments using tire chips. *Journal*
637 *of geotechnical and geoenvironmental engineering*, *123*(4), 295-304.
638 Fan, K., Zheng, Y., Baudet, B. A., & Cheng, Y. P. H. (2021). Investigation of the ultimate particle size
639 distribution of a carbonate sand. *Soils and Foundations*, *61*(6), 1708-1717.
640 Foose, G. J., Benson, C. H., & Bosscher, P. J. (1996). Sand reinforced with shredded waste tires. *Journal of*
641 *Geotechnical Engineering*, *122*(9), 760-767.
642 Fox, P. J., & Kim, R. H. (2008). Effect of progressive failure on measured shear strength of geomembrane/GCL
643 interface. Journal of Geotechnical and Geoenvironmental Engineering, 134(4), 459-469.
644 Fox, P. J., Thielmann, S. S., Sanders, M. J., Latham, C., Ghaaowd, I., & McCartney, J. S. (2018). Large-scale
645 combination direct shear/simple shear device for tire-derived aggregate. Geotechnical Testing Journal, 41(2),
646 340-353.
647 Ghazavi, M., and Sakhi, M. A. (2005). Influence of optimized tire shreds on shear strength parameters of sand.
648 International Journal of Geomechanics, 5(1), 58-65.
649 Hazarika, H., Yasuhara, K., Kikuchi, Y., Karmokar, A. K., and Mitarai, Y. (2010). Multifaceted potentials of
650 tire-derived three-dimensional geosynthetics in geotechnical applications and their evaluation. Geotextiles and
651 Geomembranes, 28(3), 303–315.
652 Humphrey D.N. (1998). Civil Engineering Applications of Tire Shreds, Manuscript Prepared for Asphalt
653 Rubber Technology Service, SC, USA.
654 Itasca. PFC Version 5.0, updated Sep 07, 2018.
655 Kim, K. S., Yoon, Y. W., & Yoon, G. L. (2011). Pull-out behavior of cell-type tires in reinforced soil
656 structures. KSCE Journal of Civil Engineering, 15(7), 1209-1217.
657 Lee, C., Shin, H., & Lee, J. S. (2014). Behaviour of sand–rubber particle mixtures: experimental
658 observations and numerical simulations. International Journal for Numerical and Analytical Methods in
659 Geomechanics, 38(16), 1651-1663.
660 Li, L. H., Chen, Y. J., Ferreira, P. M. V., Liu, Y., & Xiao, H. L. (2017). Experimental investigations on the pull-
661 out behaviour of tire strips reinforced sands. Materials, 10(7), 707.
662 Li, L., Xiao, H., Ferreira, P., and Cui, X. (2016). Study of a small scale tyre-reinforced embankment.
663 Geotextiles and Geomembranes, 44(2), 201-208.
664 Li, L., Yang, J., Xiao, H., Zhang, L., Hu, Z., & Liu, Y. (2020). Behavior of tire-geogrid-reinforced retaining
665 wall system under dynamic vehicle load. International Journal of Geomechanics, 20(4), 04020017.
666 Li, L., Fang, Y., Cheng, B., Chen, N., Tian, M., & Liu, Y. (2021). Characterisation of Geogrid and Waste
667 Tyres as Reinforcement Materials in Railway Track Beds. Materials, 14(15), 4162.
668 Lin, Y. L., Zhang, M. X., Javadi, A. A., Lu, Y., & Zhang, S. L. (2013). Experimental and DEM
669 simulation of sandy soil reinforced with H-V inclusions in plane strain tests. Geosynthetics
670 International, 20(3), 162-173.
671 Lopera Perez, J. L., Kwok, C. Y., & Senetakis, K. (2016). Effect of rubber size on the behaviour of sand-rubber
672 mixtures: A numerical investigation. Computers and Geotechnics, 80, 199-214.
673 Manohar, D. R., & Anbazhagan, P. (2021). Shear strength characteristics of geosynthetic reinforced rubber-
674 sand mixtures. Geotextiles and Geomembranes, 49(4), 910-920.
675 McCartney, J. S., Ghaaowd, I., Fox, P. J., Sanders, M. J., Thielmann, S. S., & Sander, A. C. (2017).

Shearing behavior of tire-derived aggregate with large particle size. II: Cyclic simple shear. *Journal of Geotechnical and Geoenvironmental Engineering*, *143*(10), 04017079.

Ouadfel, H., & Rothenburg, L. (2001). Stress-force-fabric relationship for assemblies of ellipsoids. Mechanics of Materials, 33(4), 201-221.

O'Shaughnessy, V. and Garga, V.K. (2000). Tire-reinforced earthfill. Part 2: Pull-out behaviour and reinforced slope design. Canadian Geotechnical Journal, 37(2), 97-116.

Ren, Z. L. (2021). Investigating the micromechanics of soil reinforced with recycled tyres using the Discrete Element Method (Doctoral dissertation, UCL (University College London)).

Ren, Z. L., Cheng, Y. P., & Xu, X. (2020). A DEM method for simulating rubber tyres. Geotechnique Letters, 10(1), 73-79.

Rothenburg, L., & Bathurst, R. J. (1989). Analytical study of induced anisotropy in idealized granular materials. Geotechnique, 39(4), 601-614.

Sayão, A.S.F.J., Gerscovich, D.M.S., Medeiros, L.V. and Sieira, A.C.C.F. (2009). Scrap tire-an attractive material for gravity retaining walls and soil reinforcement. Journal of Solid Waste Technology and Management. 35(3), 135-155.

Tran, V. D. H., Meguid, M. A., & Chouinard, L. E. (2013). A finite–discrete element framework for the 3D modeling of geogrid–soil interaction under pullout loading conditions. Geotextiles and Geomembranes, 37, 1-9.

Wang, Y. H., & Leung, S. C. (2008). A particulate-scale investigation of cemented sand behavior. Canadian Geotechnical Journal, 45(1), 29-44.

Zhang, J., Chen, X., Zhang, J., Jitsangiam, P., & Wang, X. (2020). DEM investigation of macro-and micro-mechanical properties of rigid-grain and soft-chip mixtures. Particuology, 55,128-139.